Matrix Infrared Spectra and DFT Calculations of the Reactive MH_x ($x = 1$, 2, and 3), $(H_2)MH_2$, MH_2^+, and MH_4^- (M = Sc, Y, and La) Species

Xuefeng Wang, George V. Chertihin, and Lester Andrews*

Department of Chemistry, P.O. Box 400319, University of Virginia, Charlottesville, Virginia 22904-4319

Received: May 23, 2002; In Final Form: August 5, 2002

Laser-ablated Sc, Y, and La react with molecular hydrogen to give MH, MH_2^+, MH_2, MH_3, and MH_4^- (M = Sc, Y, and La) during condensation in excess argon for characterization by matrix infrared spectroscopy. Annealing forms the dihydrogen complex $(H_2)MH_2$, which can be reduced to MH_4^- by electron capture. The (HD)MHD complex exchanges hydrogen positions on broadband photolysis to form primarily the $(D_2)MH_2$ complex. Doping the samples with CCl_4 to capture ablated electrons markedly increases the MH_2^+ infrared band intensities and decreases the MH_4^- absorptions. Further annealing produces higher $(H_2)_2MH_2$ complexes, which also exchange hydrogen positions. The reaction products are identified by deuterium and deuterium hydride isotopic substitution. DFT and MP2 theoretical calculations are employed to predict geometries and vibrational frequencies of these novel molecules, complexes, anions, and cations. Charged species from laser-ablation contribute more to the spectra of group 3 reaction products than for any other transition metal. Experiments using solid neon and pure deuterium provide complementary spectra and favor the higher $(H_2)_2$-MH_2 complexes.

Introduction

Reactions of the group 3 transition metals (Sc, Y, and La) with small molecules (O_2, CO, NO, and CO_2) have been investigated extensively in this laboratory using matrix-isolation methods.[1−6] Chemistry is very rich for the group 3 metals since their properties evolve from the reactive metals of groups 1 and 2, and charged species are a more important part of the chemistry for group 3 than any other transition metal. In addition, group 3 metals form complexes due to the availability of d orbitals. It is therefore no surprise that compounds of group 3 metals find applications in modern technology. Yttrium and lanthanum oxides play an important role in perovskite structures for high-temperature superconductivity.[7] Yttrium and lanthanum hydride films have switchable optical properties that are appropriate for a number of technological applications.[8] The electronic properties of the host metal are profoundly affected by the addition of hydrogen.[8] The nature of the solid metal trihydride ground state and mechanism of the metal−insulator transition with increasing hydrogen concentration has eluded explanation.[9,10]

Experimental studies of group 3 metal cation (Sc^+, Y^+, and La^+) reactions with hydrogen using ion beam mass spectrometry, have suggested an insertion mechanism for the primary reaction.[11,12] However, reactions of the neutral atoms with hydrogen molecules have not been investigated although emission spectra have been observed for the ScH, YH and LaH diatomic molecules.[13−19] A number of theoretical calculations have been performed for group 3 metal hydrides[20−28] mostly for the diatomic molecules. Calculations predicted the ScH_2 molecule to be linear and YH_2 and LaH_2 to be bent based on the d characters in the hybrid orbitals,[24−26] and the ScH_3 molecule was computed to be trigonal planar.[28] It is desirable to characterize these reactive metal hydride molecules by experiment.

More recently a number of transition metal hydrides and dihydrogen complexes have been investigated in low-temperature matrix samples by codeposition of laser-ablated metal atoms with molecular hydrogen in this laboratory.[29−33] Deuterium isotopic substitution and density functional theory calculations have been used to identify the reaction products. In this paper we report the infrared spectra and density functional theory calculations of MH, MH_2^+, MH_2, MH_3, $(H_2)MH_2$, $(H_2)_2MH_2$, and MH_4^- (M = Sc, Y, and La). A brief report on the homoleptic tetrametalate MH_4^- anions has been published.[34]

Experimental and Theoretical Methods

The experimental methods for reacting laser-ablated transition metal atoms with H_2 and identifying the reaction products with matrix infrared spectra have been described previously,[1,2,35,36] and the same methods are applied here for the reaction of Sc, Y, and La with H_2. Laser-ablated metal atoms were codeposited with 3−5% H_2 (D_2, HD, or $H_2 + D_2$ mixtures) in excess neon or argon and with pure deuterium onto a 3.5 K CsI window. Infrared spectra were recorded after deposition, annealing, and UV−vis irradiation. Several experiments were done with 0.1% CCl_4 added to 3% H_2 neon or argon to serve as an electron trap,[2,3,37,38] and the absorptions due to anions were reduced markedly and those due to cations were increased in the spectra of deposited samples.

DFT (density functional theory) and MP2 (Møller−Plesset) calculations of metal hydrides and metal hydride-hydrogen complexes were done for comparison with experimental results. The Gaussian 98 program[39] was employed to calculate the structures and frequencies of expected molecules. The 6-311++G(d,p) basis sets for hydrogen and scandium atoms and SDD pseudopotentials and basis sets for yttrium and lanthanum atoms were used.[40,41] All the geometrical parameters were fully optimized with either the BPW91 or B3PW91 functional (Becke nonlocal three-parameter exchange with

* To whom correspondence should be addressed. E-mail: lsa@virginia.edu.

10.1021/jp026166z CCC: $22.00
Published on Web 09/13/2002

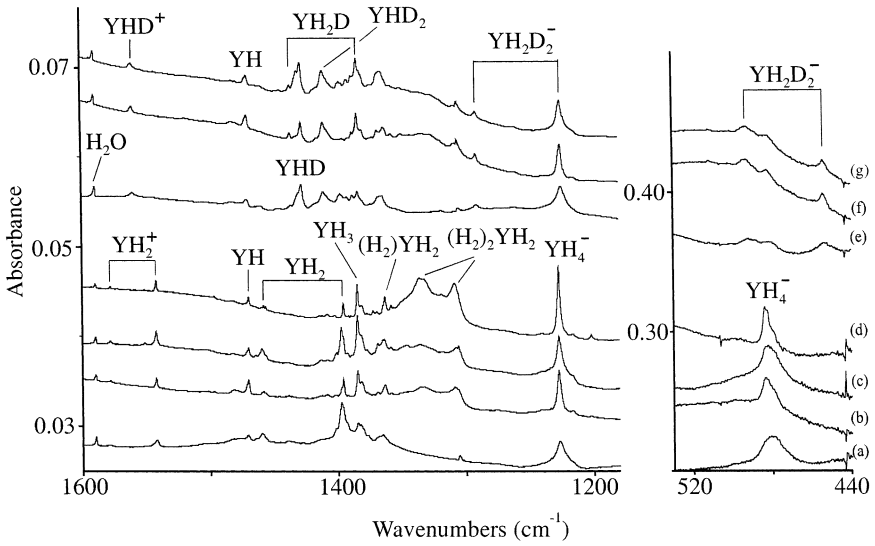

Figure 1. Infrared spectra in the 1600−1180 and 530−450 cm^{-1} regions for laser-ablated yttrium codeposited with hydrogen in argon. (a) 5% H_2 in argon deposited at 3.5 K for 60 min, (b) after annealing to 16 K, (c) after $\lambda > 240$ nm photolysis for 15 min, (d) after annealing to 25 K, (e) 5% HD in argon deposited at 3.5 K for 70 min, (f) after annealing to 16 K, and (g) after $\lambda > 240$ nm photolysis for 15 min.

PW91 functional), the B3LYP functional or ab initio calculations at MP2 level of theory.[42,43] Analytical vibrational frequencies were obtained at the optimized structures.

Results

Infrared spectra of laser-ablated Y, La, and Sc reactions with H_2 in solid argon, neon, and pure deuterium, and theoretical calculations of product molecules, complexes, and ions will be presented in turn.

Y + H_2. Matrix samples from codeposition of laser-ablated yttrium atoms with H_2, D_2, and HD in excess argon, neon, and pure deuterium at 3.5 K, with annealing and photolysis afterward, exhibit the following infrared spectral features: (i) weak bands at 1578.1, 1542.5, and 1470.4 cm^{-1} observed on codeposition with H_2 in argon and increased on annealing to 16 K. With photolysis ($\lambda > 240$ nm) the 1578.1 and 1542.5 cm^{-1} bands increased, but the 1470.4 cm^{-1} band decreased. The D_2 counterparts appeared at 1128.1, 1107.5 and 1053.1 cm^{-1}. The HD experiments gave the same 1470.4 and 1053.1 cm^{-1} bands, but different 1560.1 and 1117.9 cm^{-1} features as shown in Figures 1 and 2. With CCl_4 (0.1%) doping of H_2 (4%) in Ar, the 1578.1 and 1542.5 cm^{-1} bands increased 5-fold, but other absorptions decreased (Figure 3). Neon matrix spectra are compared in Figure 4 for group 3 metals and H_2. In neon weak 1489.4 cm^{-1} (H_2) and 1067.3 cm^{-1} (D_2) absorptions were observed, and HD spectra gave the same two bands. (ii) Two major bands at 1459.8 and 1397.8 cm^{-1} observed on deposition in argon with H_2 decreased by 60% on annealing to 16 K but recovered their intensities on photolysis. With D_2 these bands shifted to 1042.0 and 1003.2 cm^{-1}, and 1428.4 cm^{-1} in the Y−H stretching region and 1021.7 cm^{-1} in the Y−D region are the HD substitution bands. In neon similar bands at 1468.4, 1408.4 cm^{-1} (H_2) and 1050.3, 1012.0 cm^{-1} (D_2) were observed. (iii) In argon weak bands appeared at 1385.1 cm^{-1} (H_2) and 995.4 cm^{-1} (D_2) on deposition, and increased on annealing and photolysis. With HD these bands were split into three new bands: 1436.6, 1410.6, and 1384.1 cm^{-1} in the Y−H stretching region, and 1023.7, 1010.5, and 997.0 cm^{-1} in the Y−D stretching region. In the neon matrix these bands blueshifted slightly showing broad contour and strong intensities. (iv) A strong band at 1227.3 cm^{-1} with an associated band at 482.7 cm^{-1} appeared in argon on deposition, increased slightly on annealing and photolysis, but disappeared in the experiments doping with CCl_4 (Figure 3). Counterparts to the upper band were observed at 1233.3 cm^{-1} in neon and 884.4 in pure deuterium. These bands have been assigned to YH_4^- and discussed in detail.[34] (v) Broad absorptions at 1337, 1309 cm^{-1} (H_2) and 960, 943 cm^{-1} (D_2) appeared and increased on annealing. These latter bands were observed at 961, 949 cm^{-1} in solid neon along with a weak 2328 cm^{-1} associated band (Figure 5) and at 957.3, 943.8, and 2329 cm^{-1} in pure deuterium (Figure 6). The argon matrix counterpart appeared at 2315 cm^{-1} (not shown). In addition, the argon matrix solvated proton and deuteron bands were observed at 903.5 and 643.2 cm^{-1} (A = absorbance = 0.015) in these experiments.[44,45] Finally, our spectra were virtually free of metal oxide impurities as the MO bands[1−3] were very weak ($A = 0.001$).

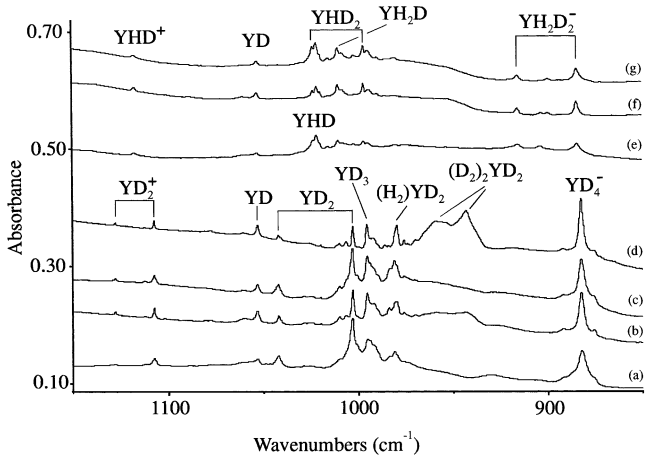

Figure 2. Infrared spectra in 1150−850 cm^{-1} region for laser-ablated yttrium codeposited with deuterium in argon. (a) 5% D_2 in argon deposited at 3.5 K for 60 min, (b) after annealing to 16 K, (c) after $\lambda > 240$ nm photolysis for 15 min, (d) after annealing to 25 K, (e) 5% HD in argon deposited at 3.5 K for 70 min, (f) after annealing to 16 K, and (g) after $\lambda > 240$ nm photolysis for 15 min.

La + H_2. Analogous experiments were done for lanthanum atom reactions with H_2, D_2, and HD in argon, and the spectra are shown in Figures 7 and 8. Strong bands at 1283.0, 1263.6, and 1114.1 cm^{-1} and weak bands at 1420.7, 1320.9, and 1235.3 cm^{-1} appeared on deposition. The 1235.3 cm^{-1} band increased

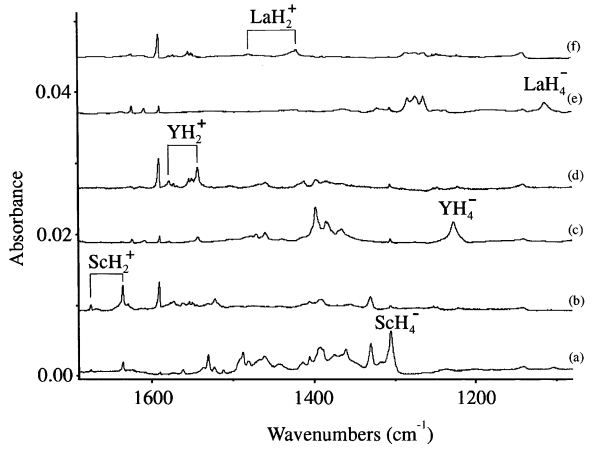

Figure 3. Infrared spectra in 1690−1080 cm^{-1} region for laser-ablated scandium, yttrium, and lanthanum codeposited with H_2 (5%) in argon doping with CCl_4 (0.1%) deposited at 3.5 K for 60 min. (a) scandium without CCl_4, (b) scandium with CCl_4, (c) yttrium without CCl_4, (d) yttrium with CCl_4, (e) lanthanum without CCl_4, and (f) lanthanum with CCl_4.

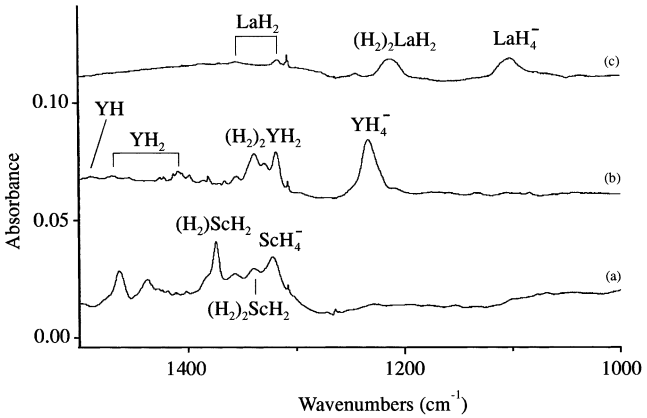

Figure 4. Infrared spectra in 1500−1100 cm^{-1} region for laser-ablated scandium, yttrium and lanthanum codeposited with hydrogen in neon deposited at 3.5 K for 60 min. (a) scandium and 5% H_2 in neon, (b) yttrium and 5% H_2 in neon, and (c) lanthanum and 5% H_2 in neon.

on annealing but decreased on photolysis with growth of the 1114.1 cm^{-1} band. Broad absorptions at 3672, 3338, 1221, and 1211 cm^{-1} appeared on later annealings. Deuterium counterparts are given in Table 2. The major product in neon is the 1101.8 cm^{-1} feature (788.7 cm^{-1} for D_2) assigned to the LaH_4^- anion[34] and a broad 1213 (863) cm^{-1} absorption, which has higher frequency associated bands at 3685, 3366 (2680, 2470) cm^{-1}. Figure 9 compares spectra for H_2, HD, and D_2 in neon. The pure deuterium spectrum reveals the former as a weak 783.2 cm^{-1} absorption and the latter as a split 863.5, 856.8 cm^{-1} feature with associated absorptions at 2684, 2681 and 2474, 2466 cm^{-1} (Figure 6).

Sc + H_2. Infrared spectra are shown in Figures 10 and 11 for laser-ablated Sc and 4% H_2, 4% D_2, and 5% HD in solid argon. Major products at 1635.8, 1530.4, 1487.7, and 1305.1 cm^{-1} and weak bands at 1391.4, 1360.9, and 1330.1 cm^{-1} were observed on deposition. The 1487.7 cm^{-1} band is particularly sensitive in the low-temperature matrix: it decreased on annealing to 18 K, but increased 4-fold on photolysis, and decreased again on further annealing. Other absorptions are given in Table 3. Absorptions at 1463.5, 1373.6, and 1321.3 cm^{-1} are the major products for Sc atom reactions with H_2 in neon on deposition, and 3676, 3400, and 1340.7 cm^{-1} features increased markedly on annealing with D_2 counterparts at 2654,

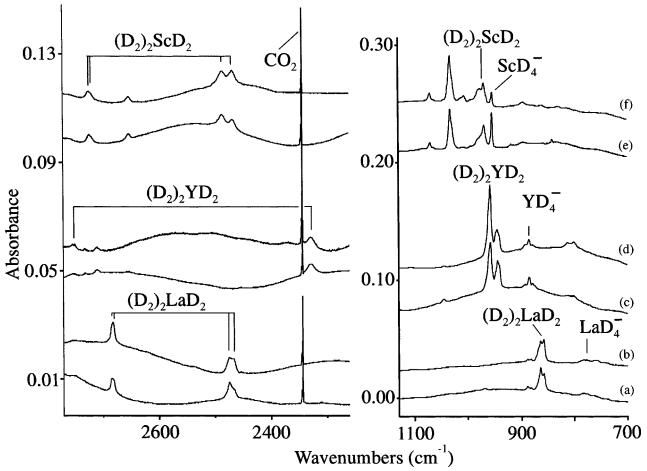

Figure 5. Infrared spectra in the 2760−2260 and 1090−750 cm^{-1} regions for laser-ablated scandium, yttrium, and lanthanum codeposited with deuterium in neon at 3.5 K for 60 min. (a) lanthanum and 2% D_2 in neon, (b) after $\lambda > 240$ nm photolysis for 15 min, (c) yttrium and 2% D_2 in neon, (d) after $\lambda > 240$ nm photolysis for 15 min, (e) scandium and 2% D_2 in neon, and (f) after $\lambda > 240$ nm photolysis for 15 min.

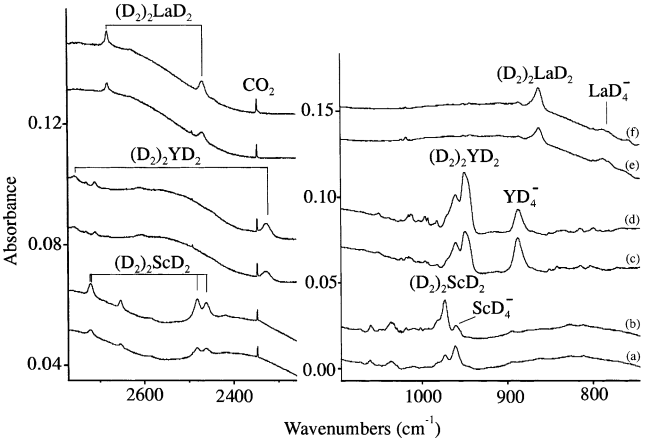

Figure 6. Infrared spectra in the 2770−2260 and 1130−700 cm^{-1} regions for laser-ablated scandium, yttrium, and lanthanum codeposited with pure deuterium. (a) scandium with pure D_2 deposited at 3.5 K, (b) after $\lambda > 240$ nm photolysis for 10 min, (c) yttrium with pure D_2 deposited at 3.5 K, (d) after $\lambda > 240$ nm photolysis for 10 min, (e) lanthanum with pure D_2 deposited at 3.5 K, (d) after $\lambda > 240$ nm photolysis for 10 min.

2462, and 973.3 cm^{-1}. In pure D_2 three strong bands at 1032.3, 968.2, and 953.4 cm^{-1} and weak bands at 2723, 2653, 2485, and 2467 cm^{-1} were observed. Spectra for the three group 3 metals in pure deuterium are compared in Figure 6.

Discussion

The new product absorptions will be assigned on the basis of argon, neon, and pure deuterium matrix spectra, isotopic shifts, isotopic splittings, and density functional theory vibrational frequency calculations.

MH. A weak absorption is observed at 1470.4 cm^{-1} after initial deposition of Y and H_2 (5%) in the argon matrix (Figure 1). With annealing to 16 K this band intensity increases 3-fold but reduces about 50% after broadband photolysis. The D_2 counterpart at 1053.1 cm^{-1} gives an isotopic ratio of 1.3963. The HD and $H_2 + D_2$ experiments reveal a clear 1470.4 and 1053.1 cm^{-1} isotopic doublet, indicating that one hydrogen atom is involved in this vibration. The above band is therefore due to the diatomic molecule YH. In solid neon YH gives a weak,

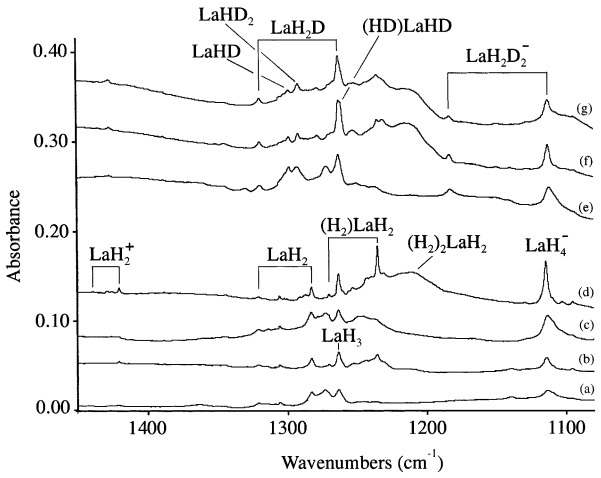

Figure 7. Infrared spectra in 1450−1080 cm^{-1} region for laser-ablated lanthanum codeposited with hydrogen in argon. (a) 5% H_2 in argon deposited at 3.5 K for 60 min, (b) after annealing to 20 K, (c) after $\lambda > 240$ nm photolysis for 15 min, (d) after annealing to 25 K, (e) 5% HD in argon deposited at 3.5 K for 70 min, (f) after annealing to 20 K, and (g) after $\lambda > 240$ nm photolysis for 15 min.

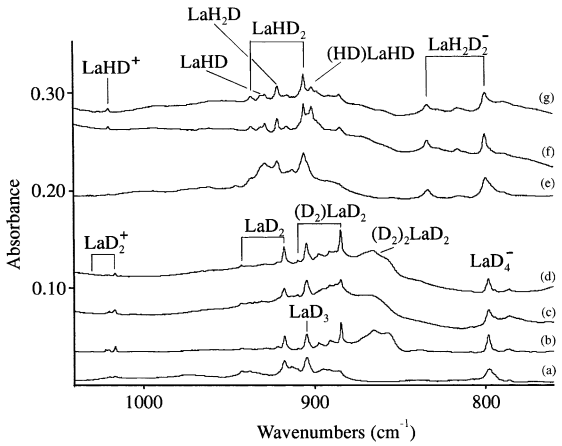

Figure 8. Infrared spectra in 1040−760 cm^{-1} region for laser-ablated lanthanum codeposited with deuterium in argon. (a) 5% D_2 in argon deposited at 3.5 K for 60 min, (b) after annealing to 20 K, (c) after $\lambda > 240$ nm photolysis for 15 min, (d) after annealing to 25 K, (e) 5% HD in argon deposited at 3.5 K for 70 min, (f) after annealing to 20 K, and (g) after $\lambda > 240$ nm photolysis for 15 min.

broad band at 1489.4 cm^{-1}, which shifts to another site at 1496.1 cm^{-1} on annealing. Absorptions for YD in neon appeared at 1067.3 and 1071.1 cm^{-1}, and the isotopic ratio is almost the same as in solid argon. The absorption for YH is excellent agreement with the gas-phase fundamental at 1491.6 cm^{-1}.[18] The yield of YH is much smaller in neon than argon matrix samples as more diffusion before solidification allows further YH reactions with H_2 to give higher hydrides. No YD is observed in pure deuterium as further reactions readily occur with D_2.

The 1530.4 cm^{-1} band observed in the Sc + H_2/Ar system has a similar fate as YH on annealing and photolysis. With D_2/Ar this band shifts to 1124.1 cm^{-1}, and with HD/Ar or H_2 + D_2/Ar the same two bands are observed at 1530.4 and 1124.1 cm^{-1}. Thus this band is assigned to ScH, which is in very good agreement with the gas phase 1547.0 cm^{-1} fundamental frequency.[17] Diatomic LaH gives a band at 1344.1 cm^{-1} in solid argon with LaD counterpart at 961.1 cm^{-1}. No gas-phase vibrational frequency[19] was obtained for LaH to compare with our matrix result, but we predict a gas-phase fundamental near 1365 cm^{-1}. Our BPW91 calculation provides a 1421 cm^{-1} harmonic fundamental, which when corrected for anharmonicity, is in good agreement with this prediction. Our BPW91 calculation also predicts a 2.064 Å bond length for the $^1\Sigma^+$ ground state, which is also in good agreement with the 2.032 Å gas-phase observation.[19]

The vibrational assignments of ScH, YH, and LaH are in accord with theoretical calculations (Table 4). The ground states are $^1\Sigma^+$ based on recent high-resolution gas-phase spectroscopy[17−19] and high-level calculations.[21−23] Our 6-311++G(d,p) basis set calculations show that two low electronic states, namely $^1\Sigma^+$ and $^3\Delta$, are very close in energy, and another $^3\Sigma^+$ state is slightly higher. For ScH the 6-311++G(3df,3pd) basis set gives 1581.4 cm^{-1} (BPW91), 1635.2 cm^{-1} (B3PW91), and 1667.5 cm^{-1} (MP2), which approach the observed ScH frequency satisfactorily. The $^1\Sigma^+$ ground state for YH is the global minimum at all levels of theory, and the results of frequency calculations are in very good agreement with observed values. MP2 calculations predict the $^1\Sigma^+$ ground state for LaH, but the $^3\Delta$ state is slightly lower in energy than the $^1\Sigma^+$ state using DFT. The LaH frequency is slightly overestimated, which is in line with the frequency predictions for ScH and YH.

Energetic laser-ablated metal atoms[46] react with molecular hydrogen to give primary MH (M = Sc, Y, and La) products, which are endothermic by 50.8 (Sc), 38.0 (Y), and 21.0 (La) kcal/mol, respectively, based on B3PW91 calculations. The increase of MH on initial annealing is due to the combination of metal atoms and hydrogen atoms trapped in the low-temperature matrix. On photolysis and further annealing, the MH absorptions decrease significantly, yielding higher order hydrides.

$$M + H_2 \rightarrow MH + H \qquad (1)$$

It is interesting to compare the H/D isotopic frequency ratios for ScH and YH in the argon matrix and in the gas phase.[17,18] The matrix ratios, 1.3870 and 1.3963, are slightly higher than the gas-phase ratios, 1.3856 and 1.3948, for ScH and YH, respectively, although the matrix shifts, 16.6 and 21.2 cm^{-1}, are reasonable.[47] The slightly higher H/D ratios suggest more hydrogen motion relative to metal, which likely arises from interaction of the argon matrix atoms with the metal center thus damping its motion and increasing its effective mass. This effect is larger for Sc where we expect a greater matrix interaction. This hypothesis is supported by the H/D ratio observed for YH/YD in solid neon, 1.3955, which is intermediate between the argon and gas-phase ratios, and the matrix interaction for neon produces a smaller 2.0 cm^{-1} shift.

ScH^+. Gas-phase reactions of Sc^+ and H_2 have been investigated extensively and the effect of Sc^+ electronic state and orbital occupation has been discussed.[11,12] The gas-phase reaction gives ScH^+, in an endothermic (47±2 kcal/mol) process, and it is likely that laser-ablated Sc^+ reacts with H_2 to give ScH^+ in these experiments as well. The sharp, weak 1561.4 cm^{-1} band, above ScH at 1530.4 cm^{-1} in solid argon, shifts to 1103.4 cm^{-1} with D_2, and the same two bands are observed with HD, which indicates the vibration of a single H(D) atom. The H/D ratio, 1.3890, is almost the same as found for ScH/ScD (1.3870). The sample doped with CCl_4 retained the 1561.4 cm^{-1} band and reduced ScH so the 1561.4 cm^{-1} band was favored relative to ScH, which is in accord with the cation assignment.[2,3,37,38]

High level ab initio calculations have determined the $^2\Delta$ ground state for ScH^+, and the $^2\Sigma^+$ state is only 1700 cm^{-1} higher, but the two states have essentially the same frequency.[48] Our DFT calculations find the ScH^+ frequency to be 55−75

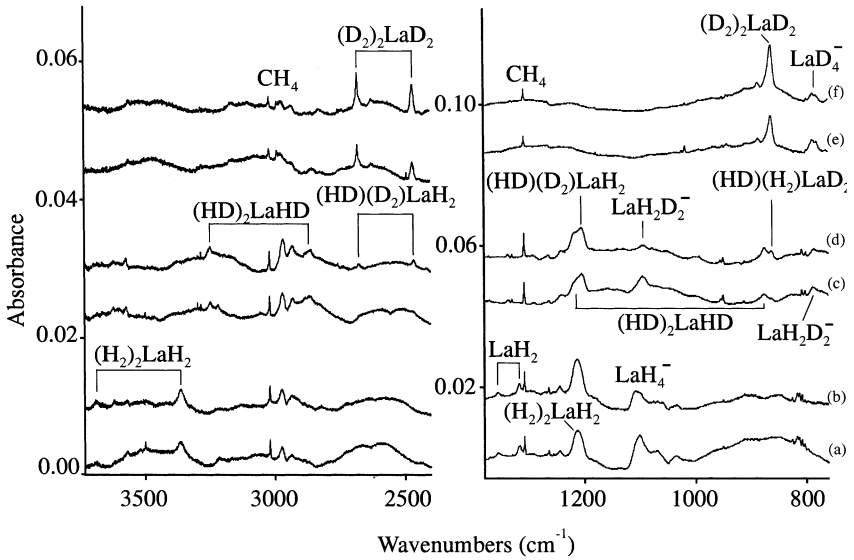

Figure 9. Infrared spectra in the 3730−2400 and 1380−760 cm^{-1} regions for laser-ablated lanthanum codeposited with isotopic hydrogen in neon at 3.5 K. (a) 2% H_2 in neon, (b) after $\lambda > 240$ nm photolysis for 15 min, (c) 2% HD in neon, (d) after $\lambda > 240$ nm photolysis for 15 min, (e) 2% D_2 in neon, and (f) after $\lambda > 240$ nm photolysis for 15 min.

TABLE 1: Infrared Absorptions (cm^{-1}) of Reaction Products of Laser-Ablated Yttrium Atom with Molecular Hydrogen in Excess Argon, Neon, and Deuterium

argon			neon			deuterium	
H_2	HD	D_2	H_2	HD	D_2	D_2	identification
					2754	2753	$(D_2)_2YD_2$
		2315		2793	2328	2329	$(D_2)_2YD_2$
1578.1	1560.1	1128.1					YH_2^+
1542.5	1117.9	1107.5					YH_2^+
			1496.1	1496.1, 1071.1	1071.1		YH site
1470.4	1470.4, 1053.1	1053.1	1489.4	1489.4, 1067.3	1067.3		YH
1459.8	1428.4	1042.0	1468.4	1438.6	1050.3	1046.5	YH_2
1397.8	1021.7	1003.2	1408.4	1030.4	1012.0		YH_2
1385.1	1436.6, 1410.6, 1383.9, 1023.7, 1010.5, 997.0	995.4					YH_3
1363.4		980.0	1381.2				$(H_2)YH_2$
1337	1334, 1308	960	1339	1337, 962	961	957.3	$(H_2)_2YH_2$
1309	962, 953	943	1318	1317, 949	949	943.8	$(H_2)_2YH_2$
	1259.8, 899.8			1265.9, 907			YHD_3^-, YH_3D^-
1227.3	1291.4, 1225.4, 915.7, 884.5	882.3	1233.3	1295.9, 1232.4, 920.5, 890.8	887.9	884.4	YH_4^-
903.5	903.5, 643.2	643.2					Ar_x^+H
482.7	492.9, 454.1						YH_4^-

TABLE 2: Infrared Absorptions (cm^{-1}) of Reaction Products of Laser-Ablated Lanthanum Atom with Molecular Hydrogen in Excess Argon, Neon, and Deuterium

argon			neon			deuterium	
H_2	HD	D_2	H_2	HD	D_2	D_2	identification
3672	3233	2674	3685	3248, 2677	2681	2681	$(H_2)_2LaH_2$
	2490	2488				2474	$(H_2)_2LaH_2$ site
3338	2950	2454, 2459	3366	2869, 2466	2468	2466	$(H_2)_2LaH_2$
1463.8	1445.2	1044.1					$(H_2)LaH_2^+$
1426.0	1032.3	1020.6					$(H_2)LaH_2^+$
1439.0	1427.4	1029.9					LaH_2^+
1420.7	1020.1	1016.6					LaH_2^+
1344.1	1344.1, 961.1	961.1					LaH
1320.9	1298.5	942.6	1355.1	1337.0	968		LaH_2
1283.0	928.4	917.6	1316.8	954.8	943.1		LaH_2
1287.1	1261.4	921.1					$(H_2)LaH_2$
1263.6	1263.0, 1292.7, 905.8, 921.3	904.5					LaH_3
1235.3	1261.2, 901.3	884.5	1246		887	887.9	$(H_2)LaH_2$
	1150.0, 816.0						$LaHD_3^-$, LaH_3D^-
1221	1218, 871	866		1220, 875		863.6	$(H_2)_2LaH_2$
1211	1231, 833 1212, 860	856	1214	1205, 863	863	856.8	$(H_2)_2LaH_2$
1114.3	1183.1, 112.4, 833.5, 799.8	797.8	1101.8	1158.5, 1096.8 825.0, 788.8	788.7	783.2	LaH_4^-

cm^{-1} higher than the ScH frequency at the BPW91 level. Given that ScH^+ is expected to red-shiftsomewhat more than ScH in the solid argon matrix,[38,47] our BPW91 calculations support assignment of the 1561.4 cm^{-1} absorption to ScH^+.

MH_2. Two bands at 1397.8 cm^{-1} (stronger) and 1459.8 cm^{-1} (weaker) tracked together on deposition of Y with H_2 in argon, decreased by 70% on annealing to 16 K, but increased 50% on broadband photolysis, and decreased on further annealing. The

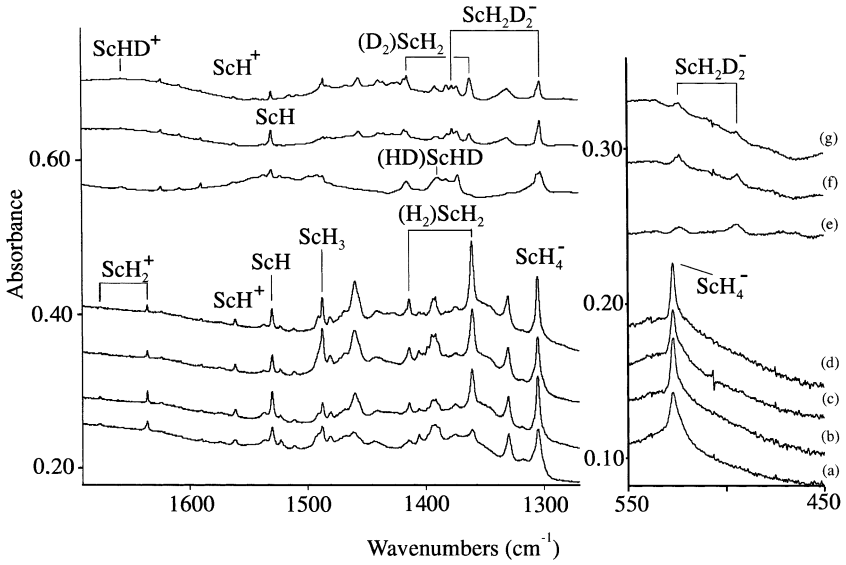

Figure 10. Infrared spectra in 1690−1270 and 550−450 cm^{-1} regions for laser-ablated scandium codeposited with hydrogen in argon. (a) 5% H_2 in argon deposited at 3.5 K for 60 min, (b) after annealing to 16 K, (c) after $\lambda > 240$ nm photolysis for 15 min, (d) after annealing to 20 K, (e) 5% HD in argon deposited at 3.5 K for 70 min, (f) after annealing to 16 K, and (g) after $\lambda > 240$ nm photolysis for 15 min.

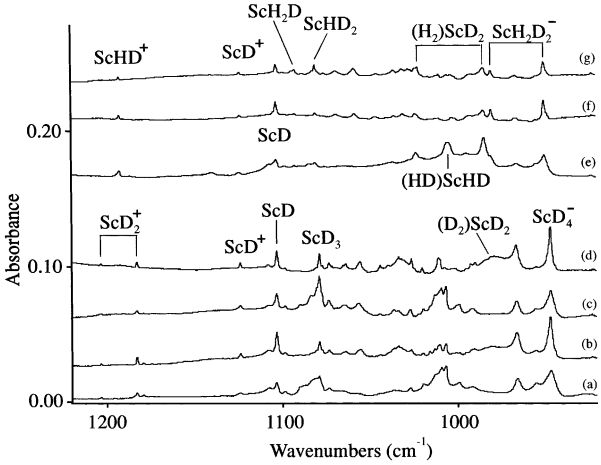

Figure 11. Infrared spectra in 1220−920 cm^{-1} region for laser-ablated scandium codeposited with deuterium in argon. (a) 5% D_2 in argon deposited at 3.5 K for 60 min, (b) after annealing to 16 K, (c) after $\lambda > 240$ nm photolysis for 15 min, (d) after annealing to 20 K, (e) 5% HD in argon deposited at 3.5 K for 70 min, (f) after annealing to 16 K, and (g) after $\lambda > 240$ nm photolysis for 15 min.

deuterium counterparts were found at 1003.2 and 1042.0 cm^{-1} giving 1.3933 and 1.4010 H/D isotopic ratios. Median bands at 1428.4 cm^{-1} (Y−H stretching region) and 1021.7 cm^{-1} (Y−D stretching region) were obtained with HD. The 1397.8 and 1459.8 cm^{-1} bands are assigned to the ν_3 and ν_1 vibrational modes for YH_2. Neon matrix counterparts were observed at 1408.4 and 1468.4 cm^{-1}.

The absorptions due to LaH_2 were observed at 1283.0 and 1320.9 cm^{-1} on deposition in the La atom reaction with H_2, which shifted to 942.6 and 917.6 cm^{-1} with D_2. The median bands at 1299.0 and 928.4 cm^{-1} are assigned to the La−H and La-D stretching vibrations in LaHD. These bands grew slightly on initial annealing (20 K) and photolysis, and decreased on further annealing (30 K). Neon matrix counterparts were weak at 1316.8 and 1355.1 cm^{-1}.

Our DFT frequency calculations support the assignments to YH_2 and LaH_2. The $^2A_1$ ground-state structures are in reasonable agreement with the previous higher level calculations.[25,26] Scale factors 0.961, 0.948 for the two modes of YH_2 and 0.951, 0.946 for the two modes of LaH_2 fit the B3PW91 frequencies to the argon matrix observations.

No absorptions for ScH_2 or ScD_2 are apparent in the infrared spectra of Sc atom reaction products with H_2 or D_2 although ScH_2 is expected to be a stable molecule similar to YH_2 and LaH_2, and we computed ScH_2 to have the same $^2A_1$ ground state (Table 5). It is likely that ScH_2 is extremely reactive with H_2 to form hydrogen complexes during matrix deposition, annealing and photolysis. Finally, the observation of ScH_4^- requires the $(H_2)ScH_2$ complex.

The insertion reactions of group 3 metals into H_2 are exothermic by 17.5 (ScH_2), 24.3 (YH_2), and 40.0 (LaH_2) kcal/mol from B3PW91 calculations. First, no spontaneous insertion reactions are observed on annealing for YH_2 and LaH_2, showing that significant activation energy is required. This is in accord with the early theoretical

$$M + H_2 \rightarrow MH_2\ (^2A_1) \qquad (2)$$

potential-energy surface investigation of MH_2 (M = Y, La), which reveals that ground-state M (^2D) has to surmount a energy barrier of 23 kcal/mol for Y and 21 kcal/mol for La for insertion into H_2 to form MH_2 ($^2A_1$).[25,26] Second, YH_2 increases significantly on broadband photolysis, so it can be deduced that photoexcited yttrium atoms surmount the energy barrier and insert into H_2. However LaH_2 is obtained only through deposition, and did not increase on photolysis. Although, we did not find any evidence for trapped ScH_2, the insertion of Sc into H_2 must happen for excess kinetic energy Sc atoms generated by laser ablation.[46] However, the insertion barrier is calculated to be 36 kcal/mol for ground-state Sc into H_2,[24] which is substantially higher than that for yttrium and lanthanum, so that once formed in these experiments, ScH_2 is highly excited and therefore very reactive.

MH_2^+. Previous gas-phase Sc^+ reactions and theoretical analysis have suggested that ScH_2^+ is formed on a singlet potential surface.[11,12,49] In the reaction of laser-ablated Sc with H_2 two bands observed at 1635.8 and 1675.2 cm^{-1} on deposition increased slightly on annealing. These bands increased in relative intensity with higher laser energy and increased 4-fold on CCl_4 doping, which point to the cation identification.[37,38] The D_2

TABLE 3: Infrared Absorptions (cm^{-1}) of Reaction Products of Laser-Ablated Scandium Atom with Molecular Hydrogen in Excess Argon, Neon, and Deuterium

argon			neon			deuterium	
H_2	HD	D_2	H_2	HD	D_2	D_2	identification
	2710	2713			2720	2723	$(H_2)ScH_2$
	2645	2645	3676		2654	2653	$(H_2)ScH_2$
	2480	2480		2480	2483	2485	$(H_2)_2ScH_2$
3400	2460	2456	3400		2462	2467	$(H_2)_2ScH_2$
1675.2	1657.4	1203.5					ScH_2^+
1635.8	1192.9	1183.0					ScH_2^+
1561.4	1561.4, 1124.1	1124.1					(ScH^+)
1530.4	1530.4, 1103.4	1103.4					ScH
1487.7	1486.2, 1514.5, 1542.6, 1092.8, 1081.1	1079.1					ScH_3
1459.8	1456.0, 1058.6	1055.7	1463.5		1060.3	1070.3	$((H_2)ScH_3)$
1414.1	1414.8, 1022.2						$(H_2)ScH_2$
1391.4	1391.3, 1010.2	1009.1			1035	1031.7	Sc_xH_y
1360.9	1362.5, 984.5 1389.5, 1004.9	(980)	1373.6		(995)		$(H_2)ScH_2$
1330.1	1330.4, 966.2	965.6	1340.7	1338.1, 979	973.3	968.0	$(H_2)_2ScH_2$
1305.1	1302.7, 1377.0, 980.2, 949.8	946.2	1321.3	1387.3, 1318.8, 992.3, 961.5	961.1	953.4	ScH_4^-
527.1	523.5, 494.2		527.6	526.6, 497.1			ScH_4^-

TABLE 4: Geometries, Vibrational Frequencies (cm^{-1}), and Infrared Intensities (km/mol) Calculated for MH (M = Sc, Y, and La)

method	state, bond (Å)	energy (kcal/mol)	frequencies, cm^{-1} (intensities, km/mol)
ScH			
BPW91/6-311++G(d,p)	$^1\Sigma^+$, 1.759	0.0	ScH: 1607.3 (230). ScD: 1149.4 (117)
	$^3\Delta$, 1.839	−6.6	ScH: 1465.5 (297). ScD: 1047.9 (152)
BPW91/6-311++G(3df,3pd)	$^1\Sigma^+$, 1.760	0.0	ScH: 1581.4 (227). ScD: 1130.8 (116)
	$^3\Delta$, 1.830	−1.2	ScH: 1455.9 (376). ScD: 1041.1 (192)
B3PW91/6-311++G(d,p)	$^1\Sigma^+$, 1.750	0.0	ScH: 1643.1 (282). ScD: 1174.9 (144)
	$^3\Delta$, 1.844	−6.7	ScH: 1482.1 (315). ScD: 1059.8 (161)
	$^3\Sigma^+$, 1.910	12.9	ScH: 1331.8 (743). ScD: 952.3 (380)
B3PW91/6-311++G(3df,3pd)	$^1\Sigma^+$, 1.750	0.0	ScH: 1635.2(280). ScD: 1169.3(143)
	$^3\Delta$, 1.844	−6.9	ScH: 1477.6(316). ScD: 1056.6(161)
MP2/6-311++G(d,p)	$^1\Sigma^+$, 1.758	0.0	ScH: 1693.4 (311). ScD: 1210.9 (159)
	$^3\Delta$, 1.907	−3.5	ScH: 1.452.8 (333). ScD: 1038.9(170)
	$^3\Sigma^+$, 1.961	51.6	ScH: 1341.2 (430). ScD: 959.1 (220)
MP2/6-311++G(3df,3pd)	$^1\Sigma^+$, 1.764	0.0	ScH: 1667.5 (316). ScD: 1192.4 (161)
	$^3\Delta$, 1.913	−3.4	ScH: 1439.8 (340). ScD: 1029.5 (174)
YH			
BPW91/6-311++G(d,p)/SDD	$^1\Sigma^+$, 1.999	0.0	YH: 1526.2 (234). YD: 1085.6 (118)
	$^3\Delta$, 1.972	7.5	YH: 1419.7 (282). YD: 1009.8 (143)
B3PW91/6-311++G(d,p)/SDD	$^1\Sigma^+$, 1.915	0.0	YH: 1554.4 (261). YD: 1105.7 (132)
	$^3\Delta$, 1.966	14.3	YH: 1434.4 (460). YD: 1020.4 (233)
	$^3\Sigma^+$, 1.966	27.0	YH: 1338.5 (748). YD: 945.0 (379)
MP2/6-311++G(d,p)/SDD	$^1\Sigma^+$, 1.918	0.0	YH: 1566.2 (312). YD: 1114.1 (158)
	$^3\Delta$, 1.985	26.4	YH: 1437.4 (322), YD: 1022.5 (163)
	$^3\Sigma^+$, 1.986	32.9	YH: 1423.6 (736). YD: 1012.7 (372)
LaH			
BPW91/6-311++G(d,p)/SDD	$^3\Delta$, 2.109	0.0	LaH: 1342.1 (432). LaD: 952.8 (217)
	$^1\Sigma^+$, 2.064	5.1	LaH: 1421.1 (294). LaD: 1008.8 (148)
	$^3\Sigma^+$, 2.156	23.2	LaH: 1258.3 (556). LaD: 893.3 (280)
B3PW91/6-311++G(d,p)/SDD	$^3\Delta$, 2.106	0.0	LaH: 1356.9 (500). LaD: 963.3 (252)
	$^1\Sigma^+$, 2.057	4.5	LaH: 1443.1 (342). LaD: 1024.5 (172)
	$^3\Sigma^+$, 2.153	23.0	LaH: 1272.5 (687). LaD: 903.4 (346)
MP2/6-311++G(d,p)/SDD	$^3\Delta$, 2.116	0.0	LaH: 1322.9 (445). LaD: 939.2 (224)
	$^1\Sigma^+$, 2.045	−11.4	LaH: 1448.2 (210). LaD: 1028.1 (101)
	$^3\Sigma^+$, 2.166	45.8	LaH: 1244.1 (903). LaD: 883.2 (455)
ScH^+	$^2\Delta$, 1.773	0.0	ScH: 1662.9 (92). ScD: 1189.2 (53)
BPW91/6-311++G(d,p)	$^2\Pi$, 1.766	−0.1	ScH: 1635.8 (219). ScD: 1169.7 (122)
	$^2\Sigma^+$, 1.744	9.0	ScH: 1657.7 (123). ScD: 1185.4 (71)
BPW91/6-311++G(3df, 3pd)	$^2\Delta$, 1.773	0.0	ScH: 1655.9 (95). ScD: 1184.1 (55)
	$^2\Sigma^+$, 1.743	8.9	ScH: 1651.8 (122). ScD: 1181.2 (70)

counterparts at 1183.0 and 1203.5 cm^{-1} and HD median absorptions at 1657.4 and 1192.9 cm^{-1} support the ScH_2^+ assignment.

With Y and H_2 in solid argon the associated bands at 1542.5 and 1578.1 cm^{-1} are assigned to the antisymmetric and symmetric Y−H stretching vibrations of YH_2^+. These bands increased on broadband photolysis and decreased on further annealing. Doping with CCl_4 to trap electrons from the ablation process enhanced the 1542.5 and 1578.1 cm^{-1} bands 5-fold, which again suggests the cation assignment.[2,3,37,38] With D_2 the two bands shifted to 1107.5 and 1128.1 cm^{-1}, respectively, giving H/D ratios 1.3928 and 1.3989. In the Y + HD experiments one band at 1560.1 cm^{-1} (Y−H stretching region) and another one at 1117.9 cm^{-1} (Y−D stretching region) were observed, which are the two stretching modes of YHD^+ from the average of the ν_3 and ν_1 frequencies of YH_2^+ and YD_2^+.

TABLE 5: Geometries, Vibrational Frequencies (cm^{-1}) and Infrared Intensities (km/mol) Calculated for MH_2 (M = Sc, Y, and La) at the B3PW91/6-311++G(d,p) Level[a]

state	geometry (angstroms, deg)	energy (kcal/mol)	frequencies, cm^{-1} (intensities, km/mol)
ScH_2			
$^2A_1$	1.816, 119.4	0.0	ScH_2: 1531.0(764, a_1), 1523.8(627, b_2), 507.5(91,a_1) ScD_2: 1095.2(327), 1090.2(393), 364.2(46) ScHD: 1527.1(688), 1093.2(368), 441.7(74)
$^2B_1$	1.886, 131.6	5.4	ScH_2: 1477.4(119,a_1), 1403.8(922,b_2), 389.8(259,a_1)
$^2A_2$	1.864, 122.1	11.2	ScH_2: 1472.8(101,a_1), 1414.5(695,b_2), 443.3(274,a_1)
$^2B_2$	1.921, 179.9	16.2	ScH_2: 1442.5(0,a_1), 1300.7(1065,b_2), 161.3(381,a_1)
YH_2			
$^2A_1$	1.955, 114.7	0.0[b]	YH_2: 1518.5 (280, a_1), 1474.3(631, b_2), 484.3(132, a_1) YD_2: 1078.1(144), 1051.1(322), 345.1(67) YHD: 1497.0(442), 1064.1(247), 420.2(102)
$^2B_1$	1.996, 117.0	16.8	YH_2: 1435.8 (365,a_1), 1396.8 (819,b_2), 454.9 (68,a_1)
$^2A_2$	1.980, 108.8	23.3	YH_2: 1439.1(217,a_1), 1396.3(516,b_2), 473.9(135,a_1)
$^2B_2$	1.999, 121.4	31.9	YH_2: 1408.7(409,a_1), 1329.3(45,b_2), 381.7(73,a_1)
LaH_2			
$^2A_1$	2.104, 109.4	0.0	LaH_2: 1388.9(494,a_1), 1355.6(774,b_2), 448.7(173,a_1) LaD_2: 984.9(251), 963.5(393), 318.8(87) LaHD: 1372.7(625), 973.8(331), 389.6(137)
$^2B_1$	2.140, 114.3	8.7	LaH_2: 1329.5(406,a_1), 1289.7(1102,b_2), 474.9(81,a_1)
$^2A_2$	2.122, 99.8	13.7	LaH_2: 1351.8(442,a_1), 1292.4(715,b_2), 385.7(111,a_1)
$^2B_2$	2.169, 122.5	33.0	LaH_2: 1261.9(618,a_1), 1112.2(4,b_2), 340.8(67,a_1)

[a] SDD used for Y and La. [b] The B3LYP functional gave 1.962 Å, 114.5°, 1506.9 cm^{-1} (259 km/mol), 1458.5 (613), and 475.9 (124).

TABLE 6: Geometries, Vibrational Frequencies (cm^{-1}), and Infrared Intensities (km/mol) Calculated for ($^1A_1$) MH_2^+ (M = Sc, Y, and La)

method	geometry (angstroms, deg)	frequencies, cm^{-1} (intensities, km/mol)
ScH_2^+		
BPW91/6-311++G(d,p)	1.737, 109.2	ScH_2^+: 1719.7(26, a_1), 1697.6 (186, b_2), 501.1(72, a_1) ScD_2^+: 1225.8(17), 1218.0(109), 359.2(44) $ScHD^+$: 1708.7(104), 1221.8(66), 436.3(64)
BPW91/6-311++G(3df,3pd)	1.735, 109.6	ScH_2^+: 1709.6(26, a_1), 1684.3(191, b_2); 497.7(68, a_1) ScD_2^+: 1218.4(17), 1208.6(112), 356.8(41) $ScHD^+$: 1697.1(106), 1213.4(67), 432.9(60)
MP2/6-311++G(d,p)	1.739, 110.1	ScH_2^+: 1845.4(64, a_1), 1774.0(565, b_2), 521.2(107, a_1) ScD_2^+: 1315.7(39), 1273.1(315), 373.6(63) $ScHD^+$: 1811.2(292), 1293.0(200), 453.4(94)
YH_2^+		
BPW91/6-311++G(d,p)/SDD	1.887, 105.4	YH_2^+: 1669.5(84, a_1), 1645.8(289, b_2); 495.3(57, a_1) YD_2^+: 1186.0(46), 1172.4(155); 352.7(32) YHD^+: 1657.8(183), 1179.1(105), 429.5(52)
BPW91/6-311++G(3df,3pd)/SDD	1.888, 105.2	YH_2^+: 1660.1(80, a_1), 1633.8(278, b_2), 487.8(54, a_1) YD_2^+: 1179.5(44), 1163.8(149), 347.3(30) YHD^+: 1647.1(175), 1171.5(101), 423.0(50)
LaH_2^+		
BPW91/6-311++G(d,p)/SDD	2.036, 106.9	LaH_2^+: 1536.4(167,a_1), 1508.1(433,b_2), 432.5(80,a_1) LaD_2^+: 1089.6(87), 1071.7(225), 307.4(42) $LaHD^+$: 1522.6(296), 1080.4(161), 375.5(68)

Very weak YH_2^+ and YD_2^+ bands are also present in HD experiments, and the YHD^+ bands were detected (4% of ν_3 mode intensities) with $H_2 + D_2$ indicating that YH_2^+ can also be formed through the combination of YH^+ and H or YH and H^+. Note that Ar_xH^+ and Ar_xD^+ were observed in all argon matrix experiments.[44,45] Neither neon nor pure deuterium traps these cations presumably owing to their great reactivity with excess hydrogen.

Likewise similar absorptions at 1420.7 and 1439.0 cm^{-1} are assigned to LaH_2^+ in the argon matrix. The D_2 absorptions shift to 1029.9 and 1016.6 cm^{-1} and the HD substituted components appeared at 1427.4 and 1020.1 cm^{-1}. The intensities of these bands are enhanced 10-fold on adding CCl_4 in H_2, HD, and D_2 experiments, confirming the cation assignment. Spectra for the three MH_2^+ cations are compared in Figure 3.

The results of BPW91 calculations for YH_2^+, LaH_2^+, and ScH_2^+ are listed in Table 6. The ground state is found to be $^1A_1$ for all three cations, and the M−H bond is predicted slightly shorter while the H−M−H bond angle is about 10° smaller than for the neutral counterpart. Strong antisymmetric stretching modes were calculated at 1697.6 (ScH_2^+), 1645.8 (YH_2^+), and 1508.1 (LaH_2^+), which are overestimated by 3.8%, 6.6%, and 6.2%, respectively, in accord with other frequency calculations for group 3 metal hydrides. Using the larger basis set (6-311++G(3df,3pd) for H gave frequencies closer to the experimental values. A red matrix shift on the order of 2% is expected for these cations in solid argon,[47] so when the observed frequencies are corrected for matrix shift the fit to calculated frequencies is better. A comparison of calculated and observed frequencies for MH_2 and MH_2^+ (M = Y and La) provides further support for these assignments. DFT calculations predict ν_1 and ν_3 of YH_2^+ 151 and 171 cm^{-1} higher than those of YH_2, whereas the observed differences are 119 and 145 cm^{-1}; for LaH_2^+, the calculated frequencies are 147 and 152 cm^{-1} higher and the observed values are 118 and 137 cm^{-1} higher.

Reactions of Sc^+ in several states with H_2 to form ScH^+ and ScH_2^+ have been explored through ab initio potential energy surfaces.[49] The M^+ cations produced here by laser ablation will

TABLE 7: Geometries, Vibrational Frequencies (cm^{-1}), and Infrared Intensities (km/mol) Calculated for ($^1A_1$) MH_3 (M = Sc, Y, and La) Molecules[a]

geometry (angstroms, deg)	frequencies, cm^{-1} (mode, intensities, km/mol)
ScH_3	
ScH: 1.820. HScH: 119.2	ScH_3: 1588.0(a_1, 3), 1517.5(e, 724 × 2), 613.9(e, 103 × 2), 113.6(a_1, 776)
	ScD_3: 1123.793), 1092.6(386 × 2), 439.7(51 × 2), 82.9(412)
	ScH_2D: 1565.8(219), 1516.8(712), 1103.5(299), 611.3(97), 506.5(69), 104.59655)
	$ScHD_2$: 1541.7(445), 1112.1(157), 1094.1(402), 559.4(81), 441.8(52), 94.3(534)
YH_3	
YH: 1.974. HYH: 113.8	YH_3: 1500.5(a_1, 40), 1441.5(e, 785 × 2), 559.0(e, 92 × 2), 262.8(a_1, 597)
	YD_3: 1062.9(22), 1028.4 × 2), 397.7(46 × 2), 188.7(308)
	YH_2D: 1481.9(262), 1441.0(773), 1039.8(319), 553.0(103), 464.9(51), 239.9(504)
	YHD_2: 1461.9(497), 1050.3(179), 1029.3(420), 504.2(86), 406.4(41), 214.6(405)
LaH_3	
LaH: 2.123. HLaH: 108.8	LaH_3: 1378.3(a_1, 140), 1320.8(e, 875 × 2), 482.2(e, 90 × 2), 328.2(a_1, 394)
	LaD_3: 976.4(72), 938.9(447 × 2), 242.2(45 × 2), 234.3(201)
	LaH_2D: 1360.3(356), 1320.7(869), 950.4(358), 474.6(112), 404.7(43), 298.3(336)
	$LaHD_2$: 1341.1(592), 962.6(229), 939.1(455), 430.8(95), 357.7(44), 264.2(259)

[a] BPW91/6-311++G(d,p) for Sc and SDD for Y and La.

include excited states. Reaction 3 is computed to be 4.4 kcal/mol exothermic for the Sc^+ reaction.[49] The M^+ reaction in the gas phase involves a similar insertion mechanism, but the MH^+ cations were characterized in the gas phase.[11,12] Here the matrix relaxes and traps the (MH_2^+) intermediate in the gas-phase H_2 reaction. The MH_2^+ cations, however, have been observed in gas-phase metal cation reactions with methane and ethane where the remaining hydrocarbon fragment assists in relaxation of the MH_2^+ cation formed.[50,51] Finally, the average bond energy[50] in ScH_2^+ is higher than that in ScH^+, which supports our stretching frequencies for ScH_2^+ being higher than that for ScH^+. In the low-temperature matrix with added CCl_4 the yields of ScH_2^+, YH_2^+, and LaH_2^+ are enhanced greatly on deposition because M^+ cations from ablation are preserved since CCl_4 served as a strong electron capture reagent.

$$M^+(^1D) + H_2 \rightarrow MH_2^+(^1A_1) \quad (3)$$

It is also interesting to note that two weak bands at 1463.8 and 1426.0 cm^{-1} appeared and increased on annealing to 25 and 30 K at the expense of LaH_2^+. The D_2 counterparts at 1044.1 and 1020.6 cm^{-1}, and HD bands at 1445.2 and 1032.3 cm^{-1} suggest a MH_2^+ vibration and the blue shift and growth on annealing infer perturbation by H_2. The $(H_2)LaH_2^+$ complex is proposed.

MH_3. A new band at 1385.1 cm^{-1} observed on deposition of laser-ablated Y with H_2 increased on annealing and doubled its intensity on broadband photolysis. The band shifted to 995.4 cm^{-1} giving a 1.3915 H/D ratio. Experiments with HD produced two triplet bands with splittings at 1436.6, 1410.6, and 1384.1 cm^{-1} in the Y−H stretching region and at 1023.7, 1010.5, and 997.0 cm^{-1} in the Y−D stretching region as shown in Figures 1 and 2. These isotopic patterns are characteristic of a metal trihydride, as found for AlH_3,[52] so YH_3 is proposed. The triplet splittings in experiments with HD are due to lowering of symmetry from C_{3v} or D_{3h} to C_{2v} or C_s. The doubly degenerate (e′) vibration (1385.1 cm^{-1} for YH_3, and 995.4 cm^{-1} for YD_3) is split into two components at 1384.1 cm^{-1} (a″) and 1436.6 cm^{-1} (a′) in YH_2D and at 997.0 cm^{-1} (a″) and 1023.7 cm^{-1} (a′) in YHD_2. Note that the (a″) component is very close to (e′) modes of YH_3 or YD_3. Moreover, the symmetric (a′) vibrations of the mixed isotopic molecules are also observed, as this mode becomes stronger than the symmetric a_1 vibration of the YH_3 or YD_3 molecules.

Similar metal trihydride bands are observed for ScH_3 and LaH_3 as listed in Tables 2 and 3. The absorptions at 1487.7 cm^{-1} for ScH_3 and at 1079.1 cm^{-1} for ScD_3 exhibit triplet splittings with HD. It is interesting to note that ScH_3 is more reactive than YH_3; ScH_3 absorption decreased on annealing and increased 3-fold on broadband photolysis. The assignment of LaH_3 is in concert with those for ScH_3 and YH_3; the 1263.6 cm^{-1} band for LaH_3 and 904.5 cm^{-1} band for LaD_3 gave a 1.3972 H/D ratio, which is the highest ratio in all three metal trihydrides. The HD band splitting also supports the trihydride assignment.

Our DFT calculations confirm these identifications of ScH_3, YH_3, and LaH_3. With the BPW91 functional the doubly degenerate (e′) modes are predicted at 1517.6 cm^{-1} for ScH_3, 1441.5 cm^{-1} for YH_3 and 1320.8 cm^{-1} for LaH_3, which are 29.9, 56.4, and 57.0 cm^{-1} too high. The computed absorptions for MH_2D and MHD_2 match the experimental data very well (Table 7). It is interesting to compare the H−M-H bond angles computed for ScH_3, YH_3 and LaH_3. It is not surprising that the M−H bond length is elongated from ScH_3 to LaH_3 because of metal size increase. The BPW91 ScH_3 calculation favors a pyramidal (C_{3v}) structure instead of planar D_{3h} even though the computed H−Sc−H bond angle is 119.2°. However, for YH_3 the H−Y−H bond angle is 113.8°, which is deviated 6.2° from the D_{3h} structure, and even more deviation is obtained for LaH_3 (108.8° for H−La−H bond angle). The nonplanar structure for ScH_3 may be an artifact of the DFT calculation as recent CCSD-(T) calculations find a D_{3h} equilibrium geometry for ScH_3 with slightly longer (1.835 Å) bond length and higher (e′) frequency (1542 cm^{-1}).[28] The CCSD(T) results validate the BPW91 frequency calculation for ScH_3 and further support the present first experimental observation of ScH_3.

The most likely mechanism for formation of MH_3 molecules is through reactions of MH with H_2, and reaction 4 is exothermic by 34.5 kcal/mol for ScH_3, 27.1 kcal/mol for YH_3, and 29.7 kcal/mol for LaH_3. Broadband photolysis promoted this reaction suggesting an energy requirement for dihydrogen activation. Further annealing allows more H_2 diffusion and molecular complexes to be formed. The broader 1459.8 cm^{-1} absorption that replaces the sharp 1487.7 cm^{-1} ScH_3 band on annealing is probably due to a $(H_2)_xMH_3$ complex.

$$MH(^1\Sigma^+) + H_2 \rightarrow MH_3(^1A_1) \quad (4)$$

$(H_2)MH_2$. The $(H_2)LaH_2$ complex was identified just below LaH_2 bands, in reactions of laser-ablated La atoms with molecular hydrogen in argon matrix experiments. The sharp absorptions at 1235.3 and 1287.1 cm^{-1}, which shift to 884.4

TABLE 8: Geometries, Vibrational Frequencies (cm^{-1}), and Infrared Intensities (km/mol) Calculated for $(H_2)MH_2$ and MH_4^- (M = Sc, Y, and La)[a]

species (symmetry, state)	geometry (angstroms, deg)	energy (kcal/mol)	frequencies, cm^{-1} (mode, intensities, km/mol)
$(H_2)ScH_2$ (C_2, ^2B)	ScH: 1.892. ScH′: 2.136. H′H′: 0.778. HScH: 143.1. H′ScH′: 23.6	0.0	3867.3(a, 36), 1456.5(a, 28), 1391.0(b, 888), 1150.8(b, 0), 616.0(a, 91), 572.1(a, 0), 490.1(a, 197), 423.8(b, 149), 223.1(b, 393)
ScH_4^- (T_d, $^1A_1$)	ScH: 1.897	−64.3	1456.2(a_1, 0), 1305.5(t_2, 1219 × 3), 525.9(t_2, 434 × 3), 520.1 (e, 0 × 2)
$(H_2)YH_2$ (C_{2v}, $^2B_1$)	YH: 1.986. YH′: 2.163. H′H′: 0.851. HYH: 117.2. H′YH′: 22.7	0.0	2755.9(a_1, 1112), 1471.2(a_1, 489), 1433.0(b_2, 889), 1251.7 (b_1, 25), 855.1(a_2, 0), 662.3(a_1, 0), 529.0(a_1, 131), 337.8(b_2, 77), 172.8(b_1, 549)
YH_4^-(T_d, $^1A_1$)	YH: 2.063	−64.5	1364.2(a_1, 0), 1241.3(t_2, 1255 × 3), 502.0(e, 0 × 2), 476.4 (t_2, 516 × 3)
$(H_2)LaH_2$ (C_{2v}, $^2B_1$)	LaH: 2.137. LaH′: 2.417. H′H′: 0.810. HLaH: 116.5. H′LaH′: 19.3	0.0	3270.7(a_1, 1165), 1339.2(a_1, 552), 1302.0(b_2, 1129), 1042.4(b_1, 38), 678.9(a_2, 0), 665.1(a_1, 2), 529.2(a_1, 128), 322.3(b_2, 61), 120.6(b_1, 628)
LaH_4^- (T_d, $^1A_1$)	LaH: 2.232	−54.6	1234.0(a_1, 0), 1118.9(t_2, 1483 × 3), 474.8(e, 0 × 2), 420.0 (t_2, 476 × 3)
$(H_2)AlH_2$ (C_s, $^2A'$)	AlH: 1.598. AlH′: 2.155. AlH″: 2.234. H′H″: 0.763. HAlH: 119.9. HAlH′: 85.4. HAlH″: 95.4	0.0	2904.0(a′, 12), 1371.4(a″, 171), 1322.8(a′, 43) 564.9(a′, 32), 522.7(a′, 97), 343.3(a′, 17), 333.0(a″, 2), 234.3(a′, 21), 118.1(a″, 0)
AlH_4^- (T_d, $^1A_1$)	AlH: 1.6494	−68.5	1726.0(a_1, 0), 1645.0(t_2, 693 × 3), 770.5(t_2, 508 × 3), 753.5(e, 0 × 2)
$(H_2)ScH_2$ (C_{2v}, $^2B_1$)	ScH: 1.855. ScH′: 2.069. H′H′: 0.807. HScH: 123.0. H′ScH′: 22.5	0.0	3290.1(a_1, 1162), 1521.3(a_1, 491), 1471.9(b_2, 887), 1149.4(b_1, 2), 742.9(a, 54), 614.7(a_2, 0), 495.9(a_1, 117), 295.8(b_2, 54), 205.4(b_1, 518)
ScH_4^- (T_d, $^1A_1$)	ScH: 1.897	−60.2	1463.7(a_1, 0), 1311.4(t_2, 1217 × 3), 529.5(t_2, 434 × 3), 529.6 (e, 0 × 2)
$(H_2)YH_2$ (C_{2v}, $^2B_1$)	YH: 1.993. YH′: 2.184. H′H′: 0.840. HYH: 117.1. H′YH′: 22.2	0.0	2837.6(a_1, 1142), 1464.9(a_1, 478), 1424.8(b_2, 852), 1217.8 (b_1, 21), 821.5(a_2, 0), 665.3(a_1, 0), 524.2(a_1, 120), 328.8(b_2, 70), 145.0(b_1, 577)
YH_4^- (T_d, $^1A_1$)	YH: 2.067	−68.1	1362.9(a_1, 0), 1239.3(t_2, 1246 × 3), 512.1(e, 0 × 2), 479.9 (t_2, 479 × 3)
$(H_2)LaH_2$ (C_{2v}, $^2B_1$)	LaH: 2.149. LaH′: 2.450. H′H′: 0.820. HLaH: 116.2. H′LaH′: 18.8	0.0	3354.6(a_1, 1515), 1331.2(a_1, 551), 1291.7(b_2, 1110), 1009.4(b_1, 42), 669.5(a_2, 0), 633.1(a_1, 1), 515.6(a_1, 121), 306.9(b_2, 57), −64.5(b_1, 748)
LaH_4^- (T_d, $^1A_1$)	LaH: 2.243	−57.9	1226.4(a_1 0), 1110.2(t_2, 1471 × 3), 481.6(e, 0 × 2), 420.2(t_2, 453 × 3)
$(H_2)AlH_2$ (C_s, $^2A'$)	AlH: 1.597. AlH′: 2.278. AlH″: 2.373. H′H″: 0.756. HAlH: 119.4. HAlH′: 84.8. HAlH″: 94.2	0.0	4210.3(a′, 18), 1881.2(a″, 339), 1841.3(a′, 82) 752.9(a′, 193), 668.4(a′, 60), 432.4(a′, 26), 409.3(a″, 2), 220.5(a′, 35), 160.9(a″, 0)
AlH_4^- (T_d, $^1A_1$)	AlH: 1.646	−71.2	1732.8(a_1, 0), 1646.3(t_2, 714 × 3), 782.2(t_2, 535 × 3), 361.8(e, 0 × 2)

[a] Using 6-311++G(d,p) for Sc and SDD for Y and La. Top block used B3PW91 and bottom block B3LYP functionals.

and 921.3 cm^{-1} with D_2, are due to the ν_3 and ν_1 vibrational modes for the LaH_2 moiety in $(H_2)LaH_2$ and LaD_2 in $(D_2)LaD_2$, respectively. These bands appeared on annealing, disappeared on photolysis, and restored on further annealing. With HD two median bands for the LaHD subunit were observed at 1261.2 and 901.2 cm^{-1}; however, bands due to the LaH_2 and LaD_2 moieties also appeared with the same behavior, indicating the exchange of inequivalent hydrogen from (HD)LaHD to (D_2)-LaH_2 or $(H_2)LaD_2$. The growth of $(D_2)LaH_2$ is substantially more than $(H_2)LaD_2$ as the former is lower in total energy by 0.5 kcal/mol and the latter is higher by 0.4 kcal/mol than (HD)-LaHD owing to zero point energy.

Likewise, similar absorptions were observed for $(H_2)YH_2$ at 1363.4 cm^{-1} and for $(D_2)YD_2$ at 980.0 cm^{-1}. With HD new bands due to $(D_2)YH_2$ at 1366 cm^{-1} and $(H_2)YD_2$ at 980 cm^{-1} appeared owing to hydrogen exchange with the former an order of magnitude stronger. Finally, $(D_2)YH_2$ is lower than (HD)-YHD by 0.4 kcal/mol whereas $(H_2)YD_2$ is higher by 0.3 kcal/mol owing to zero point energy and this affects the partition among the mixed isotopic complexes.

The analogous complex, $(H_2)ScH_2$, must be formed since the ScH_4^- electron capture product is observed in these matrix samples, but the assignment of specific bands is not straightforward because different structures appear to be favored for $(H_2)ScH_2$ and $(D_2)ScD_2$. The HD reaction gives evidence for (HD)ScHD in solid argon, which rearranged to both $(D_2)ScH_2$ and $(H_2)ScD_2$ on annealing and photolysis in favor of the former isotopic molecule. Table 3 lists the possible absorptions for (H_2)-ScH_2, which may be trapped in twisted C_2 or C_{2v} structures as B3PW91 and B3LYP calculations converged these structures, respectively.

DFT calculations were performed for $(H_2)MH_2$ (M = Sc, Y, and La) to determine the frequencies, vibrational intensities, and isotopic distributions (Table 8). The predicted ν_3 and ν_1 modes of the MH_2 subunits are 1391.0, 1456.5 cm^{-1} for $(H_2)ScH_2$, 1433.0, 1471.2 cm^{-1} for $(H_2)YH_2$, and 1302.0, 1339.2 cm^{-1} for $(H_2)LaH_2$, which are in line with the experimental results of 30−50 cm^{-1} red shifts for MH_2 relative to $(H_2)MH_2$. Thus, it appears that most of the ScH_2 formed in these experiments is trapped as $(H_2)ScH_2$. Reaction 5 is exothermic by 6.6, 2.3 and 0.6 kcal/mol (B3PW91) for Sc, Y, and La, respectively. This is sufficient to activate the exchange of side-bonded complexed (H_2) and metal hydride (MH_2) positions as $(D_2)ScH_2$ results from (HD)ScHD formed on annealing and photolysis (Figs. 10,11). It should be noted that these $(H_2)MH_2$ complexes are relatively weak, based on the computed H′−H′ bond lengths. For comparison the computed H−H length in $Pd(H_2)$, 0.854 Å,[29] exceeds all of the present complex values. We do not observe the H−H stretching mode for the $(H_2)MH_2$ complexes although our DFT calculations predict sizable intensity. Our experience is that calculations overestimate the H−H mode intensity[29] and that these bands are broad makes them more difficult to detect.

$$H_2 + MH_2\,(^2A_1) \rightarrow (H_2)MH_2 \qquad (5)$$

MH_4^-. With La and H_2 a band at 1114.3 cm^{-1} appeared on deposition, increased on annealing and photolysis. Assignment to the antisymmetric La−H stretching mode in LaH_4^- is

substantiated by D_2 and HD substitution.[34] With D_2 the 1114.3 cm^{-1} band shifts to 797.8 cm^{-1} and with HD the 1114.3 cm^{-1} band splits into 1183.1 and 1112.4 cm^{-1}, and the 797.8 cm^{-1} band into 833.5 and 799.8 cm^{-1}. The observation of four stretching modes (two La−H and two La−D) confirms that this is a tetrahydride species.[53] These bands are eliminated by doping with CCl_4, which preferentially captures electrons and thus identifies an anion species.[2,3,37,38] In neon the La−H and La−D stretching modes in LaH_4^- and LaD_4^- appeared at 1101.8 and 788.7 cm^{-1}, respectively, and a similar isotopic splitting pattern was observed for $LaH_2D_2^-$. In contrast the isoelectronic HfH_4 molecule has much higher frequencies (1678.3 and 630.7 cm^{-1})[53] and the intervening lanthanide series contraction and relativistic effects[54] for hafnium are not manifest for lanthanum compounds. The ScH_4^- and YH_4^- analogues have been identified in solid argon, neon, and deuterium on the basis of similar spectroscopic observations.[34] The H/D ratios for the ν_3 modes increase for ScH_4^-, YH_4^-, and LaH_4^-, respectively, from 1.3793 to 1.3910 to 1.3965 as the heavier metal contributes less to the reduced mass of the vibration. We note that the same $MH_2D_2^-$ anions were observed with the HD and the mixed $H_2 + D_2$ reagents, which demonstrates that all H(D) positions in this tetrametalate anion are equivalent. As can be seen in Figure 6, the anion yield decreases in the series $ScD_4^- > YD_4^- > LaD_4^-$ in solid deuterium.

The $(H_2)MH_2$ complexes are formed spontaneously from combination of MH_2 and H_2 (reaction 5). Electrons are abundant in the laser ablation process and $(H_2)MH_2$ can electron capture to give the tetrametalate anion MH_4^-. Broadband irradiation also contributes electrons for reaction 6 particularly in the case of lanthanum.

$$(H_2)MH_2 + e^- \rightarrow MH_4^- \quad (6)$$

The observation of weak M−H and M−D stretching modes for Y and La in MHD_3^- and MH_3D^- in HD experiments requires exchange through the higher order $(HD)_2MHD$ complex, which after rearrangement to $(H_2)(HD)MD_2$ or $(D_2)(HD)MH_2$ photodissociates (D_2) or (H_2) and then electron captures to form the MHD_3^- or MH_3D^- anions. Likewise the YHD_3^- and YH_3D^- bands were detected in the $H_2 + D_2$ experiments, which also requires exchange through the higher order isotopic complexes. Furthermore, electron capture is sufficiently exothermic to expell the extra dihydrogen ligand.

$$(H_2)_2MH_2 + e^- \rightarrow MH_4^- + H_2 \quad (7)$$

Here electron affinity plays an important role in the formation of the metal tetrahydride anions. Electron affinities estimated from DFT, 2.79 eV for $(H_2)ScH_2$, 2.80 eV for $(H_2)YH_2$, and 2.37 eV for $(H_2)LaH_2$, are substantial and only slightly lower than the 2.97 eV value for $(H_2)AlH_2$ using the B3PW91 functional and 2.61, 2.95, 2.51 and 3.08 eV for group 3 and Al, respectively, using B3LYP. Close agreement for these two functionals validates the calculation. The stable isolated AlH_4^- anion is prepared by UV irradiation (240 nm) of Al and the $(H_2)AlH_2$ complex in solid argon.[55] The electron affinity of $(H_2)AlH_2$ more than makes up for the difference between the photon energy and the ionization energy of Al atom. Similar laser-ablation experiments give isolated AlH_4^- in solid argon at 1609.0 cm^{-1}, in excellent agreement with the photolysis experiments of Manceron et al.[55] Calculated structures and frequencies for $(H_2)AlH_2$ and AlH_4^- are also given in Table 8 for comparison. Finally, the BH_4^- anion is more stable than the analogous $(H_2)BH_2$ complex by 3.07 eV, calculated for the equilibrium structures, and both are observed in similar neon matrix experiments.[56]

$(H_2)_2MH_2$ Absorptions. A broad band at 1221, 1211 cm^{-1} in La + H_2 argon experiments and weak associated 3672 and 3338 cm^{-1} absorptions shift to 866, 856 cm^{-1} and 2674 and 2459 cm^{-1} with D_2. These bands increase on late annealing and are appropriate for the higher $(H_2)_2LaH_2$ complex. The observation of two H−H (D−D) stretching modes requires the bisdihydrogen complex of $LaH_2(LaD_2)$ with a lower La−H_2-(D_2) stretching mode. The H/D ratios, 1.373 and 1.351, are appropriate for H−H (D−D) stretching modes with considerable anharmonicity. This identification is substantiated by the pure deuterium matrix experiment where splittings in each band (2684, 2681 cm^{-1}, 2474, 2466 cm^{-1}, and 863.6, 856.8 cm^{-1}) coordinate on annealings and photolysis. The neon matrix counterparts are particularly interesting as nearly the same 2681, 2468, and 863 cm^{-1} absorptions are observed (Figure 5). In addition to $(HD)_2LaHD$ at 3248, 2869, 1220, and 863.3 cm^{-1}, HD in neon gave two new bands at 2677 and 2466 cm^{-1} for D−D stretching modes, the 1205 cm^{-1} La−H_2 absorption for this complex was much stronger than the 856.8 cm^{-1} La−D_2 absorption, and photolysis favored the new products. This again indicates rearrangement of hydrogen positions in $(HD)_2LaHD$ to give $(HD)(D_2)LaH_2$ and in addition that the dihydrogen ligands are inequivalent. We suggest that the more strongly bonded D_2 absorbs at 2466 cm^{-1} in $(HD)(D_2)LaH_2$ and the less strongly bonded D_2 absorbs at 2677 cm^{-1} in $(D_2)(HD)LaH_2$ in solid neon. Finally, with $H_2 + D_2$ we observed the 2681 and 2468 cm^{-1} bands for the D−D stretching modes and the dominant 1202 cm^{-1} band for the La−H_2 stretching mode in the $(D_2)_2LaH_2$ complex.

In the Y + H_2 product spectra broad bands at 1337 and 1309 cm^{-1} with deuterium counterparts at 960 and 943 cm^{-1} in argon are due to the Y−H(D) stretching vibration in higher dihydrogen complexes, most likely $(H_2)_2YH_2$, and a weak 2315 cm^{-1} band is due to the stronger of two D−D stretching modes. These bands increased on late annealing and decreased on photolysis. With HD the Y−H counterpart bands at 1334 and 1308 cm^{-1} are much stronger than the Y−D stretching bands at 962 and 953 cm^{-1}, suggesting that hydrogen position exchange occurs in these complexes favoring the $(D_2)(HD)YH_2$ form, as found for the (HD)MHD complexes. In neon the bands at 1339 and 1318 cm^{-1} and at 961 and 949 cm^{-1} and a weak 2328 cm^{-1} band are the major product absorptions besides YH_4^-. The two Y−H_2(D_2) stretching modes are probably due to different structures trapped in the matrix.

Absorptions at 3400 and 1300 cm^{-1} are attributed to the $(H_2)_2ScH_2$ complex, and bands at 2480, 2456, and 965.6 cm^{-1} follow for the $(D_2)_2ScD_2$ complex. The $(D_2)_2ScH_2$ argon matrix band at 1330 cm^{-1} is much stronger than the $(H_2)_2ScD_2$ band at 966 cm^{-1}; the strong D−D stretching 2480, 2460 cm^{-1} band is observed with HD, again substantiating the exchange of hydrogen positions in these complexes. Similar results were obtained with HD in neon. The D−D stretching absorptions are illustrated for neon and deuterium matrix experiments in Figures 5 and 6.

DFT calculations for $(H_2)_2YH_2$ and $(H_2)_2LaH_2$ provide some support for the identification of these complexes although these results are only approximate. We were not able to converge structures for $(H_2)_2ScH_2$ nor with equivalent H_2 ligands. These calculations suggest that one of the dihydrogen ligands is bound more strongly than the other, the former gives a strong infrared absorption, and the M−H_2 modes are red-shifted from $(H_2)MH_2$ values. Calculations are given in Table 9 for the yttrium

TABLE 9: Geometries, Vibrational Frequencies (cm^{-1}), and Infrared Intensities (km/mol) Calculated for $(H_2)_2MH_2$ (M = Y and La)

species (symmetry state)	geometry (angstroms, deg)	frequencies, cm^{-1} (intensities, km/mol)
$(H_2)_2YH_2$ (C_{2v}, $^2B_1$)	YH: 1.995. YH′:2.172. YH″: 2.291. H′H′: 0.843. H″H″: 0.781. HYH: 128.5	3801.2(a_1, 12), 2849.1(a_1, 1398), 1435.9(a_1, 279), 1407.0(b_2, 868), 1256.9(b_1, 0), 1150.8(b_2, 0), 837.7(a_1, 4), 792.3(a_2, 0), 722.5(a_1, 85), 641.1(a_2, 0), 537.4(a_1, 1), 507.6(b_2, 171), 250.8(b_1, 422), 247.8(b_2, 17), 192.2(b_1, 71)
$(H_2)_2LaH_2$ (C_{2v}, $^2B_1$)	LaH: 2.10. LaH′: 2.448. LaH″: 2.472. H′H′: 0.802. H″H″: 0.776. HLaH: 122.8	3875.5(a_1, 14), 3387.0(a_1, 1769), 1315.1(a_1, 349), 1290.9(b_2, 1045), 1049.9(b_2, 4), 1026.0(b_1, 1), 725.6(a_1, 59), 694.9(a_2, 0), 652.5(a_2, 0), 636.2(a_1, 23), 499.9(a_1 4), 435.1(b_2, 161), 271.4(b_1, 322), 230.8(b_2, 14), 169.0(b_1, 222)

[a] B3PW91/6-311++G(d,p)/SDD) for H and SDD for Y and La.

and lanthanium species. As found for $Pd(H_2)_{1,2,3}$ complexes[29] the intensities of H−H ligand vibrations are overestimated.

Other Absorptions. The 1391.4 cm^{-1} band with Sc in argon is favored by higher laser energy and photolysis. This band and the 1009.1 cm^{-1} D_2 counterpart show little shift with HD substitution. A higher metal species is suggested.

Conclusions

Laser-ablated group 3 atoms react with H_2 to form MH, MH_2^+, MH_2, MH_3, $(H_2)MH_2$, and MH_4^- (M = Sc, Y, and La), which are identified in solid argon. The diatomic molecules give absorptions at 1530.4 cm^{-1} for ScH, 1470.4 cm^{-1} for YH, and 1344.1 cm^{-1} for LaH, which further react with H_2 to produce the metal trihydrides, MH_3, that absorb at 1487.7 cm^{-1} for ScH_3, 1385.1 cm^{-1} for YH_3, and 1263.8 cm^{-1} for LaH_3. The dihydrides were observed at 1459.8 and 1397.8 cm^{-1} for YH_2, and at 1320.9 and 1283.0 cm^{-1} for LaH_2, but no absorptions due to ScH_2 were identified. It is likely that ScH_2 is extremely reactive and further reaction with H_2 occurs during formation of the low-temperature matrix.

Dihydrogen−metal hydride complexes, $(H_2)MH_2$, are also produced as H_2 is coordinated to MH_2, which are analogous to $(H_2)RhH_2$, $(H_2)AuH$, and $(H_2)PtH$.[21−23] The $(H_2)MH_2$ complexes are labile and exchange hydrogen positions readily on formation during annealing as shown for (HD)ScHD rearrangement to $(D_2)ScH_2$ and $(H_2)ScD_2$. Such dihydrogen complexes may be involved in the uptake of H_2 in solid group 3 metal hydride films.[8]

The $(H_2)MH_2$ complexes electron capture to give the stable tetrametalate anions MH_4^-, which absorb at 1305.1, 527.1 cm^{-1} for ScH_4^-, 1227.3, 482.7 cm^{-1} for YH_4^-, and 1114.3 cm^{-1} for LaH_4^-. These absorptions are eliminated by doping with CCl_4, which preferentially captures ablated electrons. The MH_4^- anions are identified from two M−H_2 and two M−D_2 vibrational modes using the HD reagent, and the same spectrum with HD and $H_2 + D_2$ mixtures shows that these anions are homoleptic. The tetrametalate anions are sufficiently stable in these experiments to suggest preparation on a larger scale for use as reducing agents.

Similar experiments in neon and pure deuterium, however, give higher hydride $(H_2)_2MH_2$ complexes as the major products owing to the greater diffusion range of dihydrogen during the neon condensation process. These $(H_2)_2MH_2$ complex absorptions increase markedly on late annealing in argon and exhibit strong M−H_2 stretching modes and two weak absorptions for the dihydrogen ligands (H_2, HD, and D_2 counterparts). The $(HD)_2MHD$ complexes also exchange hydrogen positions on annealing and photolysis.

The group 3 dihydride cations were observed in the low-temperature argon matrix from the H_2 reaction with laser-ablated M^+ cations. Weak bands at 1675.2 and 1635.8 cm^{-1} for ScH_2^+, 1578.1 and 1542.5 cm^{-1} for YH_2^+, and 1439.0 and 1420.7 cm^{-1} for LaH_2^+ are due to the ν_1 and ν_3 modes of the bent cations. These absorptions are substantially enhanced in CCl_4 doping experiments since M^+ concentrations are maintained owing to CCl_4 serving as a capture reagent for electrons. Charged species contribute more to the spectra of group 3 reaction products than for any other transition metal. Although solid neon works better than solid argon for the trapping of charged species in many systems, this is not the case for the small reactive group 3 metal dihydride cations, which undergo more reactions during the slower condensation process in solid neon.

Acknowledgment. We gratefully acknowledge support for this work from N.S.F Grant CHE 00-78836 and early experiments performed by G. P. Kushto.

References and Notes

(1) Chertihin, G. V.; Andrews, L.; Rosi, M.; Bauschlicher, C. W., Jr. *J. Phys. Chem. A* **1997**, *101*, 9085 (Sc+O_2).
(2) Andrews, L.; Zhou, M.; Chertihin, G. V.; Bauschlicher, C. W., Jr. *J. Phys. Chem. A* **1999**, *103*, 6525 (Y, La+O_2).
(3) Bauschlicher, C. W., Jr.; Zhou, M.; Andrews, L.; Johnson, J. R. T.; Panas, I.; Snis, A.; Roos, B. O. *J. Phys. Chem. A* **1999**, *103*, 5463 (Sc+O_2).
(4) Zhou, M.; Andrews, L. *J. Phys. Chem. A* **1999**, *103*, 2964.
(5) Kushto, G. P.; Zhou, M.; Andrews, L.; Bauschlicher, C. W., Jr. *J. Phys. Chem. A* **1999**, *103*, 1115.
(6) Zhou, M.; Andrews, L. *J. Am Chem. Soc*. **1998**, *120*, 13230.
(7) Bednorz, J. G.; Muller, K. A.; Takashige, M. *Science* **1987**, *236*, 73.
(8) Huiberts, J. N.; Griessen, R.; Rector, J. H.; Wijngaarden, R. J.; Dekker, J. P.; de Groat, D. G.; Koeman, N. J. *Nature* **1996**, *380*, 231.
(9) Shinar, J.; Dehner, B.; Barnes, R. G.; Beaudry, B. J. *Phys. Rev. Lett.* **1990**, *64*, 563.
(10) Vajda, P.; Daou, J. N. *Phys. Rev. Lett.* **1991**, *66*, 3176.
(11) Elkind, J. L.; Armentrout, P. B. *J. Phys. Chem*. **1987**, *91*, 2037.
(12) Elkind, J. L.; Sunderlin, L. S.; Armentrout, P. B. *J. Phys. Chem*. **1989**, *93*, 3151.
(13) Smith, R. E. *Proc. R. Soc. Lon. Ser. A* **1973**, *332*, 113.
(14) Bernard, A.; Effantin, C.; Bacis, R. *Can. J. Phys*. **1977**, *55*, 1654.
(15) Bernard, A.; Bacis, R. *Can. J. Phys.* **1976**, *54*, 1509.
(16) Bernard, A.; Bacis, R. *Can. J. Phys.* **1977**, *55*, 1322.
(17) Ram, R. S.; Bernath, P. F. *J. Chem. Phys.* **1996**, *105*, 2668.
(18) (a) Ram, R. S.; Bernath, P. F. *J. Chem. Phys*. **1994**, *101*, 9283. (b) Ram, R. S.; Bernath, P. F. *J. Mol. Spectrosc*. **1995**, *171*, 169.
(19) Ram, R. S.; Bernath, P. F. *J. Chem. Phys.* **1996**, *104*, 6444.
(20) Pyykko, P. *Phys. Scr*. **1979**, *20*, 647.
(21) (a) Bauschlicher, C. W., Jr.; Walch, S. P. *J. Chem. Phys.* **1982**, *76*, 4560. (b) Langhoff, S. R.; Pettersson, L. G. M.; Bauschlicher, C. W., Jr.; Partridge, H. *J. Chem. Phys.* **1987**, *86*, 268.
(22) (a) Balasubramanian, K.; Wang, J. Z. *J. Mol. Spectrosc*. **1989**, *133*, 82. (b) Das, K. K.; Balasubramanian, K. *Chem. Phys. Lett.* **1990**, *172*, 372.
(23) Anglada, J.; Bruna, P. J.; Peyerimhoff, S. D. *Mol. Phys.* **1989**, *66*, 541 and references therein.
(24) Balasubramanian, K. *Chem. Phys. Lett*. **1987**, *135*, 288.
(25) Balasubramanian, K.; Ravimohan, C. *Chem. Phys. Lett*. **1988**, *145*, 39.
(26) Das, K. K.; Balasubramanian, K. *J. Phys. Chem.* **1991**, *95*, 42.
(27) (a) Neuhaus, A. H.; Glendening, E. D.; Streitwieser, A. *Organometallics* **1996**, *15*, 3688. (b) Fujii, T. S.; Iwata, S. *Chem. Phys. Lett*. **1996**, *251*, 150.
(28) Balabanov, N. B.; Boggs, J. E. *J. Phys. Chem. A* **2000**, *104*, 1597.
(29) Andrews, L.; Wang, X.; Alikhani, M. E.; Manceron, L. *J. Phys. Chem. A* **2001**, *105*, 3052 (Pd+H_2).
(30) Andrews, L.; Wang, X.; Manceron, L. *J. Chem. Phys.* **2001**, *14*, 1559 (Pt+H_2).

(31) Wang, X.; Andrews, L. *J. Am. Chem. Soc*. **2001**, *123*, 12899 ($Au+H_2$).
(32) Wang, X.; Andrews, L. *J. Phys. Chem*. **2002**, *106*, 3706 ($Rh+H_2$).
(33) Wang, X.; Andrews, L. *J. Am. Chem. Soc*. **2002**, *124*, 5636 (WH_6).
(34) Wang, X.; Andrews, L. *J. Am. Chem. Soc*. **2002**, *124*, 7610 (Sc, Y, LaH_4^-).
(35) Burkholder, T. R.; Andrews, L. *J. Chem. Phys.* **1991**, *95*, 8697.
(36) Hassanzadeh, P.; Andrews, L. *J. Phys. Chem*. **1992**, *96*, 9177.
(37) (a) Zhou, M. F.; Andrews, L. *J. Am. Chem. Soc*. **1998**, *120*, 11499. (b) Zhou, M. F.; Andrews, L. *J. Am. Chem. Soc*. **1999**, *121*, 9171.
(38) Zhou, M. F.; Andrews, L.; Bauschlicher, C. W., Jr. *Chem. Rev.* **2001**, *101*, 1931 (M+CO).
(39) Frisch, M. J.; Trucks, G. W.; Schlegel, H. B.; Scuseria, G. E.; Robb, M. A.; Cheeseman, J. R.; Zakrzewski, V. G.; Montgomery, J. A., Jr.; Stratmann, R. E.; Burant, J. C.; Dapprich, S.; Millam, J. M.; Daniels, A. D.; Kudin, K. N.; Strain, M. C.; Farkas, O.; Tomasi, J.; Barone, V.; Cossi, M.; Cammi, R.; Mennucci, B.; Pomelli, C.; Adamo, C.; Clifford, S.; Ochterski, J.; Petersson, G. A.; Ayala, P. Y.; Cui, Q.; Morokuma, K.; Malick, D. K.; Rabuck, A. D.; Raghavachari, K.; Foresman, J. B.; Cioslowski, J.; Ortiz, J. V.; Stefanov, B. B.; Liu, G.; Liashenko, A.; Piskorz, P.; Komaromi, I.; Gomperts, R.; Martin, R. L.; Fox, D. J.; Keith, T.; Al-Laham, M. A.; Peng, C. Y.; Nanayakkara, A.; Gonzalez, C.; Challacombe, M.; Gill, P. M. W.; Johnson, B.; Chen, W.; Wong, M. W.; Andres, J. L.; Gonzalez, C.; Head-Gordon, M.; Replogle, E. S.; Pople, J. A. *Gaussian 98*, revision A.6, Gaussian, Inc.: Pittsburgh, PA, 1998.
(40) (a) Krishnan, R.; Binkley, J. S.; Seeger, R.; Pople, J. A. *J. Chem. Phys*. **1980**, *72*, 650. (b) Frisch, M. J.; Pople, J. A.; Binkley, J. S. *J. Chem. Phys*. **1984**, *80*, 3265.
(41) Andrae, D.; Haussermann, U.; Dolg, M.; Stoll, H.; Preuss, H. *Theor. Chim. Acta* **1990**, *77*, 123.
(42) (a) Becke, A. D. *J. Chem. Phys*. **1993**, *98*, 5648. (b) Perdew, J. P.; Wang, Y. *Phys. Rev. B* **1992**, *45*, 13244.
(43) (a) Møller, C.; Plesset, M. S. *Phys. Rev*. **1934**, *46*, 618. (b) Binkley, J. S.; Pople, J. A. *Int. J. Quantum Chem*. **1975**, *9*, 229.
(44) Milligan, D. E.; Jacox, M. E. *J. Mol. Spectrosc*. **1973**, *46*, 460.
(45) Andrews, L.; Ault, B. S.; Grzybowski, J. M.; Allen, R. O. *J. Chem. Phys.* **1975**, *62*, 2461.
(46) Kang, H.; Beauchamp, J. L. *J. Phys. Chem.* **1985**, *89*, 3364.
(47) Jacox, M. E. *Chem. Phys.* **1994**, *189*, 149.
(48) Pettersson, L. G. M.; Bauschlicher, C. W., Jr.; Lanehoff, S. R.; Partridge, H. *J. Chem. Phys.* **1987**, *87*, 481.
(49) Rappé, A. K.; Upton, T. H. *J. Chem. Phys.* **1986**, *85*, 4400.
(50) Sunderlin, L.; Aristov, N.; Armentrout, P. B. *J. Am. Chem. Soc.* **1987**, *109*, 78.
(51) Sunderlin, L. S.; Armentrout, P. B. *J. Am. Chem. Soc.* **1989**, *111*, 3845.
(52) Chertihin, G. V.; Andrews, L. *J. Phys. Chem.* **1993**, *97*, 10295.
(53) (a) Chertihin, G. V.; Andrews, L. *J. Am. Chem. Soc*. **1995**, *117*, 6402. (b) Chertihin, G. V.; Andrews, L. *J. Phys. Chem*. **1995**, *99*, 15004. (c) Wang, X.; Andrews, L. To be published.
(54) Pyykkö, P. *Chem. Rev*. **1988**, *88*, 563.
(55) Pullumbi, P.; Bouteiller, Y.; Manceron, L. *J. Chem. Phys*. **1994**, *101*, 3610.
(56) Andrews, L.; Wang, X. *J. Am. Chem. Soc.* **2002**, *124*, 7280 ($B+H_2$).